Journal Name

COMMUNICATION

$Bi_2Fe_4O_9$ thin films as novel visible-light-active photoanodes for solar water splitting

Received 00th January 20xx,
Accepted 00th January 20xx

DOI: 10.1039/x0xx00000x

www.rsc.org/

Yaqiong Wang,[a] Matyas Daboczi,[b] Camilo A. Mesa,[c] Sinclair Ryley Ratnasingham,[a,d] Ji-Seon Kim,[b] James R. Durrant,[c] Steve Dunn,[*e] Haixue Yan,[a] and Joe Briscoe [*a]

We report the chemical solution deposition (CSD) of a phase-pure $Bi_2Fe_4O_9$ thin film for use as a photoanode in photoelectrochemical (PEC) water splitting. The energy levels of $Bi_2Fe_4O_9$ films have been measured and n-type characteristics have been confirmed. With band gaps determined as 2.05 eV (indirect) and 2.80 eV (direct) and valence and conduction bands straddling the water oxidation and reduction potentials, this material is highly promising as a photocatalyst for solar water splitting. The photocurrent of a planar photoanode reached 0.1 mA/cm² at 1.23 V_{NHE} under AM1.5 G illumination. The addition of H_2O_2 as a hole scavenger increased the photocurrent to 0.25 mA/cm², indicating hole injection is one limiting factor to the performance. The performance was enhanced by nearly 5-fold when the $Bi_2Fe_4O_9$ photoanode is coupled to a Co-Pi surface co-catalyst. The photoanode also shows excellent stability with no change in photocurrent over three hours of continuous illumination. These results indicate that this material represents a promising addition to the growing selection of low-cost, stable photocatalysts for use in solar water splitting.

Novel materials for efficient solar-to-fuel conversion have been pursued extensively since the first report of water oxidation using TiO_2[1, 2]. Along with TiO_2, other binary transition metal oxides such as Fe_2O_3[3, 4] and WO_3[5], have been explored and found to show many desirable properties for the production of solar fuels. However, these materials usually have some limitations either from large optical band gaps or short carrier diffusion lengths[6, 7]. For example, the application of TiO_2 is significantly limited by a large band gap of *ca* 3.2 eV, which means only 3 – 4% of solar light can be used to generate photoexcited carriers. Efforts have been made to address these challenges such as doping to reduce the band gap[8] or nanostructuring to overcome the short carrier diffusion lengths[9]. Meanwhile, increasing research attention has been paid to the development of ternary metal oxides for application as photoanodes. The materials of interest include narrow-band-gap $BiVO_4$[10] and $CuWO_4$[11] as well as those with polar structures such as $BaTiO_3$[12] and $PbZr_xTi_{1-x}O_3$[13].

It is worth noticing that many compounds containing Bi^{3+} have been found to be narrow-band-gap semiconductors. In addition these Bi^{3+} containing compounds can show high PEC activity under visible light due to the strong hybridization between O-2p and Bi-6s orbitals[14, 15]. It has also been found that hybridized energy bands can increase the separation of photoexcited holes and electrons and further improve the PEC conversion efficiency[16]. Therefore, in addition to $BiVO_4$, other Bi-based compounds, $CuBi_2O_4$[17], $BiFeO_3$[18], and Bi_2WO_6[19] have attracted interest as possible visible-light photocatalysts.

$Bi_2Fe_4O_9$ has attracted attention for a number of applications such as semiconductor gas sensors and catalyst for ammonia oxidation to NO[20]. Like many other Bi-based compounds, $Bi_2Fe_4O_9$ exhibits a narrow indirect band gap with reported values ranging from ca. 1.9 to ca. 2.1 eV[21, 22]. Nanoparticles of $Bi_2Fe_4O_9$ have been reported to be highly visible-light-active photocatalysts with a near-infrared absorption. These particles show good photocatalytic activity for organic contaminant degradation[23]. However, to date there has been no reported studies on the use of $Bi_2Fe_4O_9$ thin films as photoelectrodes for PEC applications.

In this work, we prepare $Bi_2Fe_4O_9$ thin films using chemical solution deposition (CSD) and study the photoelectrochemical performance of the as-produced thin films. The $Bi_2Fe_4O_9$ electrode exhibits photoanodic behaviour with high PEC activity and good stability under simulated sunlight. A photocurrent density of 0.1 mA/cm² at 1.23 V_{NHE} was obtained under AM1.5G

[a] School of Engineering and Materials Science and Materials Research Institute, Queen Mary University of London, Mile End Road, London E1 4NS, United Kingdom. *j.briscoe@qmul.ac.uk
[b] Department of Physics and Centre for Plastic Electronics, Imperial College London, South Kensington, London, SW7 2AZ, UK
[c] Department of Chemistry, Imperial College London, South Kensington Campus, London SW7 2AZ, United Kingdom
[d] Department of Materials and Centre for Plastic Electronics, Imperial College London, South Kensington, London, SW7 2AZ, UK
[e] School of Engineering, London South Bank University, 103 Borough Road, London, SE1 0AA, United Kingdom.*dunns4@lsbu.ac.uk

† Electronic Supplementary Information (ESI) available: details of experimental procedures; Kelvin probe; UV-APS; SPV measurements; Faradaic efficiency additional data; Co-Pi deposition data; stability in 1 M KOH. See DOI: 10.1039/x0xx00000x

irradiation. A value of 0.05 mA/cm^2 was obtained when the UV light was blocked, demonstrating the ability of $Bi_2Fe_4O_9$ to harvest visible light for photochemical reactions. The addition of a hole scavenger (H_2O_2) in the PEC process increased the photocurrent to 0.25 mA/cm^2 at 1.23 V_{NHE} and lowered the onset potential. Based on these results, we propose that $Bi_2Fe_4O_9$ is a promising photoanode for PEC applications.

$Bi_2Fe_4O_9$ thin films were deposited using a simple CSD using a stoichiometric 1:2 molar ratio of bismuth nitrate and iron nitrate as precursors in a sol which also contained 2-methoxyethanol and acetic anhydride. Five layers of the sol were spin coated onto fluorine-doped tin oxide coated glass substrates, with staged drying and annealing up to a maximum of 650 ℃ (full methods in Supplementary Information). Figure 1a shows a typical surface scanning-electron microscope (SEM) micrograph for the $Bi_2Fe_4O_9$ thin films showing smooth films with grains from 50 – 200 nm. Figure 1b shows a cross-section of a typical film indicating that the film is *ca.* 150 nm thick and consists of several small crystallites. X-ray diffraction pattern of the as-produced film (Figure 1c) confirms that a phase-pure sample of $Bi_2Fe_4O_9$ has been produced with an orthorhombic structure (ICDD 74-1098; space group: *Pbam*) and lattice constants of a = 7.950 Å, b = 8.428 Å, and c = 6.005 Å. All additional peaks in the diffraction pattern can be attributed to the substrate.

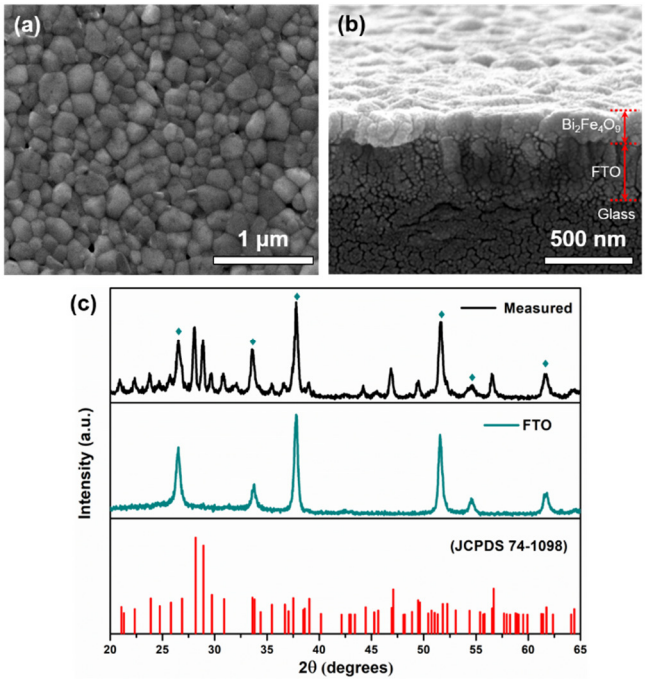

Figure 1. a) Top-down and b) cross-section SEM images of the $Bi_2Fe_4O_9$ film. c) XRD pattern of the $Bi_2Fe_4O_9$ film (measured), with the measured pattern of the FTO substrate, and reference spectrum for $Bi_2Fe_4O_9$ (JCPDS 74-1098) for comparison. Sample peaks corresponding to the FTO substrate are indicated. All other peaks index to $Bi_2Fe_4O_9$.

X-ray photoelectron spectroscopy (XPS) was undertaken to characterize the elemental composition and chemical states of the $Bi_2Fe_4O_9$ film. The XPS spectra of a typical sample is shown in Figure 2, with the XPS full survey spectrum shown in Figure 2a. All obtained binding energies were normalized using the C 1s peak at 284.6 eV. A detailed view of the bismuth 4f spectrum is given in Figure 2b and shows two distinct peaks: the Bi $4f_{7/2}$ peak at 158.9 eV and the Bi $4f_{5/2}$ peak at 164.2 eV. Both these peaks and their positions are characteristic of the presence of bismuth in the +3 oxidation state, as expected for $Bi_2Fe_4O_9$.

The Fe 2p core level, shown in Figure 2c, consists of two peaks located at 723.7 eV (Fe $2p_{1/2}$) and 710 eV (Fe $2p_{3/2}$). The Fe $2p_{3/2}$ peak was deconvoluted into two peaks located at 711.1 eV and 709.6 eV, corresponding to Fe^{3+} and Fe^{2+}, respectively. The formation of Fe^{2+} is attributed to the presence of oxygen vacancies commonly occurring in the deposition processes of perovskite thin films[24, 25], which is further confirmed in the O 1s spectrum: the deconvolution of the O 1s line results in peaks at 529.5 eV and 531.5 eV. The peak at 529.5 eV belongs to M-O-M bonds and that at 531.5 eV is due to a high number of defect sites with a low oxygen coordination, i.e. due to the presence of oxygen vacancies in accordance with the presence of Fe^{2+}.

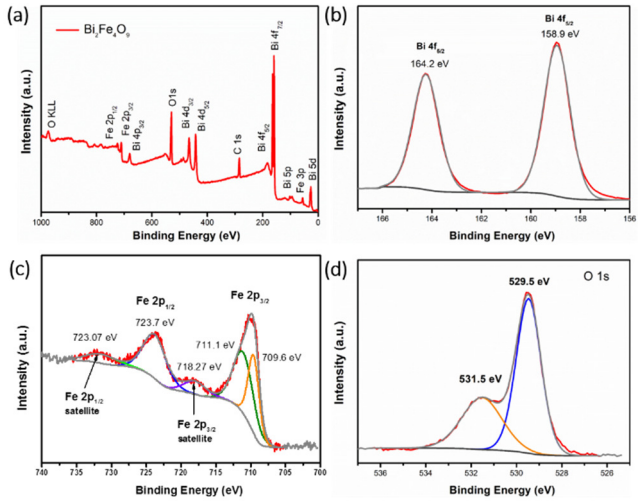

Figure 2. (a) Survey spectrum, (b) Bi 4f, (c) Fe 2p and (d) O 1s XPS spectra of $Bi_2Fe_4O_9$ film showing fitted peaks.

The UV-vis absorption spectrum of the $Bi_2Fe_4O_9$ films shown in Figure 3a demonstrates light absorption over a wide range of frequencies from the UV into the visible, consistent with the reported band gap of around 2 eV. It has been reported in previous studies that the $Bi_2Fe_4O_9$ nanoparticle samples had near-infrared light absorption, which was ascribed to the splitting of Fe 3d transitions[26]. For our thin film samples a broad, shallow absorption peak can be observed between 650 nm to 800 nm, and a distinct absorption edge starts from ~ 600 nm and increases with the decreasing wavelength. The good visible light absorption of the material indicates the possibility of photoactivity under visible-light illumination.

The linear regions in the derived Tauc plots (Figure 3b) indicate indirect and direct band gaps of 2.05 eV and 2.80 eV respectively, in close agreement with the calculated band structure for $Bi_2Fe_4O_9$[27]. The band gap associated with the indirect transition is close to ideal for solar water splitting[28], giving an indication that the material will be able to drive photochemical processes under visible light. However, the

indirect transition means that there will be limited light absorption across the thin sample and gives some indication as to why nanoparticles have been of interest to date: the absorption cross section and scattering associated with nanoparticles can add to the effective pathlength and increase absorption. Despite this, the presence of a direct transition at an only slightly higher energy of 2.8 eV means that there is still strong absorption within the visible region, as seen in the absorption spectrum (Figure 3a).

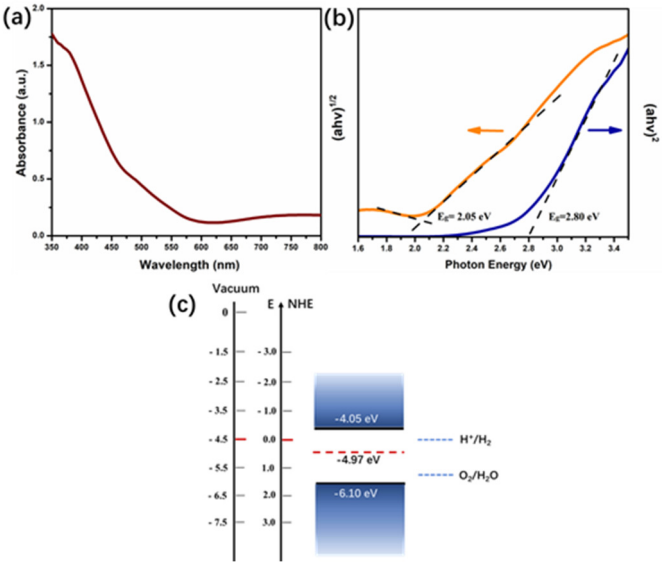

Figure 3. a) UV-vis absorbance spectra and b) derived Tauc plots corresponding to the allowed direct (right scale) or allowed indirect (left scale) band gap. c) Energy levels of $Bi_2Fe_4O_9$ electrode. Red dashed line shows the measured Fermi level. The redox potentials of water splitting are also shown

To understand the variety of photochemistry that can be driven on the surface of a photocatalyst the band structure of the system must be understood, particularly in the case of a relatively new material as reported here. In order to obtain the energy levels of the $Bi_2Fe_4O_9$ films, UV ambient pressure photoemission spectroscopy[29] (UV-APS) and Kelvin probe measurement have been carried out to determine the valence-band edge and the Fermi energy level (E_F). The measured valence-band edge by UV-APS is -6.10 eV and the measured E_F value is - 4.97 eV. Note that the constant E_F value was measured over 100s indicating a stable electronic property of the $Bi_2Fe_4O_9$ films. Based on these values and the measured indirect optical band gap energy of 2.05 eV, a band diagram was constructed (shown in Figure 3c), indicating $Bi_2Fe_4O_9$ is slightly n-doped and has a valence band edge below the water oxidation potential, suitable for photocatalytic water oxidation. The n-type characteristic of the material was also confirmed by surface photovoltage measurements[30, 31], which show a negative shift in work function upon illumination (Fig. S3, ESI).

The photoanodic activity of $Bi_2Fe_4O_9$ films were investigated using PEC in a standard three electrode configuration. Figure 4a shows the photocurrent-voltage (J-V) curves of a $Bi_2Fe_4O_9$ photoelectrode illuminated using full AM1.5G and visible light only (λ > 420 nm) chopped irradiation. The data shows a steady increase in photocurrent with increasing applied anodic potential and the photocurrent at 1.23 V_{NHE} reached 0.1 mA/cm^2 under full sun illumination. Despite the large number of previous studies of PEC water oxidation using bismuth ferrite films with composition $BiFeO_3$, this has produced consistently lower photocurrent values than our $Bi_2Fe_4O_9$ thin films. For example, Yu *et al.*[32] produced for $BiFeO_3$ films deposited by pulsed laser deposition (PLD) and obtained ~ 0.09 mA/cm^2 at 1.23 V_{NHE} under 1 sun, which was higher than that reported by Quynh[33] who also prepared $BiFeO_3$ by PLD giving ~0.06 mA/cm^2 at 1.1 V_{NHE} under 1 sun. A $BiFeO_3$ film deposited on epitaxial $SrRuO_3/SrTiO_3$ substrate by sputtering has been reported to have a much lower value of ~ 0.01 mA at 1 V_{NHE}[18]. It is worth noting that the $Bi_2Fe_4O_9$ photoanode reported here was prepared by a low-cost deposition method and is a planar film without nanostructuring. It therefore offers a large scope to further optimise the synthesis and morphology of this material to produce improved photocurrent in the future, along similar lines as the well-studied photoanode material: Fe_2O_3. This has demonstrated photocurrents over 2 mA/cm^2 (at 1.23 V_{NHE}) through the production of optimised nanostructured films[3, 4, 34], while planar films – more directly comparable to the $Bi_2Fe_4O_9$ photoanode reported herein – generally produce negligible photocurrents, or those in the low μA/cm^2 range[35].

To confirm the visible-light response of the $Bi_2Fe_4O_9$ thin films, photocurrent was measured with the UV portion filtered from the AM1.5G illumination (λ > 420 nm), which reached 0.05 mA/cm^2 at 1.23 V_{NHE}, confirming the potential for $Bi_2Fe_4O_9$ to be a visible-light-active catalyst indicated by the UV-Vis spectra.

It can be seen from Figure 4a that the chopped light J-V curves showed obvious transient photocurrent peaks upon light switching. Such peaks are known to be associated with a variation in the rates of carrier extraction across the semiconductor interface[36]. To investigate this in more detail we have studied the impact of a hole-scavenger, H_2O_2, on the photocurrent of the system. Figure 4b shows a plot of current density vs applied potential under chopped illumination using two different electrolytes: 0.2 M Na_2SO_4 and 0.2 M Na_2SO_4-0.5 M H_2O_2. The onset potential for the photocurrent shifted negatively with the addition of H_2O_2 to the electrolyte solution (from 0.7 to 0.3 V_{NHE}). This agrees well with the expectation, since H_2O_2 has a more negative oxidation potential than H_2O (E^0 = +0.68 V_{NHE} for O_2/H_2O_2 and E^0 = +1.23 V_{NHE} for O_2/H_2O), which means that the E^0_{redox} of the two electrolyte solutions are 0.34 V_{NHE} (with H_2O_2) and 0.615 V_{NHE} (without H_2O_2).

The transient photocurrents associated with the non-equilibrium extraction of holes and electrons have also been significantly reduced upon the addition of H_2O_2 and the photocurrent at 1.23 V_{NHE} increased to 0.25 mA/cm^2. Transient photocurrents under chopped illumination have been observed in a range of photoanode materials such as Fe_2O_3[36] and $BiVO_4$[37]. This phenomenon has been associated with a characteristic signature of hole accumulation at the photoanode/electrolyte interface[38]. The kinetics of the 4-hole oxidation of water to molecular oxygen means that there is an excess of generation of photoexcited holes over the rate of extraction to perform the electrochemical reaction. It is accepted that positive current

transients upon turning the light on represent the accumulation of holes at the electrode/electrolyte interface. A negative current transient observed upon turning the light off represents the back reaction of electrons from the conduction band with the accumulated holes[36]. The addition of H_2O_2 as a hole scavenger promotes the reaction of accumulated holes at the electrode/electrolyte interface and suppresses back electron-hole recombination. The addition of a hole scavenger demonstrates that the photocurrents of $Bi_2Fe_4O_9$ electrode can be further improved in the future by eliminating the hole injection barrier at the electrode/electrolyte interface, for example by combination with co-catalysts or reduction in surface trap states.

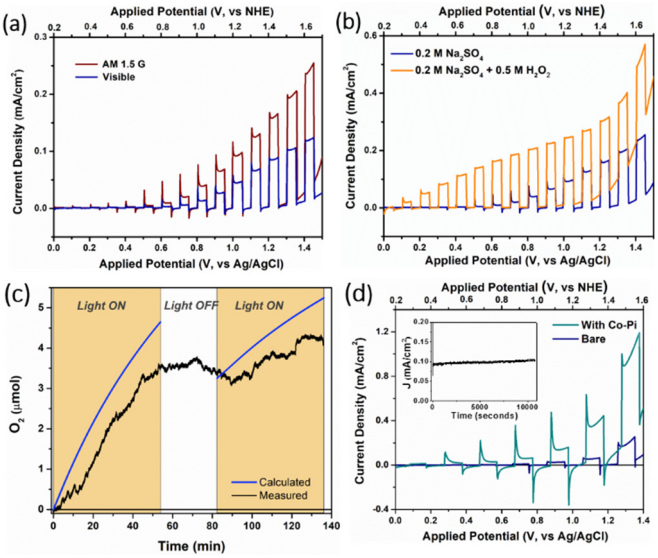

Figure 4. a) J-V curve for $Bi_2Fe_4O_9$ under both chopped 100 mW/cm² AM 1.5 G and visible light irradiation (λ > 420 nm) in Na_2SO_4 electrolyte (pH 6.5). b) J-V curve under chopped illumination (1 sun AM 1.5 G) for $Bi_2Fe_4O_9$ electrode without and with a hole scavenger (H_2O_2). c) Oxygen evolution measured by a Clark electrode in gas phase (black) and the amount of oxygen calculated (blue) from the chronoamperometry. d) Chopped J-V curve for $Bi_2Fe_4O_9$ electrode without and with Co-Pi co-catalyst deposition. Inset: Photocurrent density (J) – time curves of $Bi_2Fe_4O_9$ electrode measured at an applied potential of 1.2 V_{NHE} for 3h in 0.2 M Na_2SO_4 solution under 1 sun illumination indicating good stability.

The ability of the photoanode to produce oxygen under illumination was measured using a Clark electrode (full details in ESI). It can be seen from Figure 4c that the measured oxygen content clearly increases over the periods of illumination, indicating successful photoelectrocatalytic water oxidation. Furthermore, the Faradaic efficiency (FE) for oxygen evolution was calculated by comparing this measured oxygen evolution to the theoretical maximum oxygen production, derived from the chronoamperometry (at 1.2 V vs. Ag/AgCl; full details of the calculation method are given in the ESI). This gave a FE of 82.1 ± 5.9 %. This is remarkably high compared to other ferrites ($BiFeO_3$) that have shown FE close to 70%[39], again indicating the promise of this system as a potential high-efficiency photoanode material.

Considering the issues with hole accumulation and associated recombination discussed above, co-catalyst deposition was investigated as a route to enhance the performance of the $Bi_2Fe_4O_9$ photoanode. A CoO_x overlayer (Co-Pi) was deposited on the surface of the $Bi_2Fe_4O_9$ (details of method in ESI) and chopped light J-V was re-tested. As shown in Figure 4d, the deposition of the Co-Pi overlayer shifts the photocurrent onset potential ~ 200 mV to more negative potentials as well as the dark onset. Although transient photocurrent spikes are still present, indicating high levels of hole accumulation and recombination, the addition of the Co-Pi increases the photocurrent density by approximately a factor of 5, indicating it is a promising route to enhance the photoelectrocatalytic performance of this material, as found with other systems.

A key consideration for the use of photocatalytic materials is the stability of the system under illumination. We studied the stability of a $Bi_2Fe_4O_9$ electrode by measuring the photocurrent over time (chronoamperometry) under an applied potential of 1.2 V_{NHE} and full sunlight illumination in a 0.2 M Na_2SO_4 electrolyte (as used in all previous measurements), as shown in Figure 4d (inset). It can be seen from the J-t results that there is no loss of photocurrent during the 3-hour test, indicating the good stability of $Bi_2Fe_4O_9$ films under illumination for use as a photoanode. The stability was also tested under illumination in 1 M KOH (commonly used for photoanode testing), and the $Bi_2Fe_4O_9$ films were also stable for at least three hours with no drop in photocurrent (see Figure S7 in the ESI), indicating that this materials should be photostable under operating conditions ranging from pH 6.5 to pH 14.

Conclusions

We present the first report of the use of $Bi_2Fe_4O_9$ as a photoanode for photoelectrochemical water oxidation. Phase-pure $Bi_2Fe_4O_9$ films have been synthesized via a simple CSD method using a stoichiometric Bi/Fe molar ratio of 1:2 for the precursor preparation. The $Bi_2Fe_4O_9$ photoanode exhibits an indirect bandgap of 2.05 eV coupled with a direct transition at 2.8 eV leading to a strong visible light response. The measured band positions indicate suitability for water oxidation. PEC tests demonstrate high activity of the $Bi_2Fe_4O_9$ electrode under AM1.5G and visible light illumination. By adding a hole scavenger, we have demonstrated that a hole injection barrier exists at the surface of the $Bi_2Fe_4O_9$ electrode. This indicates that the PEC performance of the material can be further improved by combination with other photo- or electrocatalysts, or other tools such as modification of surface states to enhance carrier extraction, or nanostructuring to increase active surface area. We show that $Bi_2Fe_4O_9$ combines strong light absorption, easy fabrication and good stability under illumination, making it a promising candidate for photoanodes in application of practical solar energy-driven PEC water splitting.

Conflicts of interest

There are no conflicts to declare

Acknowledgements

Y.W. would like to acknowledge Chinese Scholarship Council for supporting this work. The authors acknowledge the UK EPSRC for the Plastic Electronics Centre for Doctoral Training (EP/G037515/1) and KP Technology for a CASE studentship. C.A.M. acknowledges COLCIENCIAS (call 568) for funding.

Notes and references

1. A. Fujishima and K. Honda, *Nature*, 1972, **238**, 37.
2. C. X. Kronawitter, L. Vayssieres, S. Shen, L. Guo, D. A. Wheeler, J. Z. Zhang, B. R. Antoun and S. S. Mao, *Energy & Environmental Science*, 2011, **4**, 3889-3899.
3. D. A. Wheeler, G. Wang, Y. Ling, Y. Li and J. Z. Zhang, *Energy & Environmental Science*, 2012, **5**, 6682-6702.
4. A. Kay, I. Cesar and M. Grätzel, *Journal of the American Chemical Society*, 2006, **128**, 15714-15721.
5. J. A. Seabold and K.-S. Choi, *Chemistry of Materials*, 2011, **23**, 1105-1112.
6. P. S. Bassi, Gurudayal, L. H. Wong and J. Barber, *Physical Chemistry Chemical Physics*, 2014, **16**, 11834-11842.
7. K. Sivula and R. van de Krol, *Nature Reviews Materials*, 2016, **1**, 15010.
8. R. Asahi, T. Morikawa, T. Ohwaki, K. Aoki and Y. Taga, *science*, 2001, **293**, 269-271.
9. H.-J. Ahn, M.-J. Kwak, J.-S. Lee, K.-Y. Yoon and J.-H. Jang, *Journal of Materials Chemistry A*, 2014, **2**, 19999-20003.
10. T. W. Kim and K.-S. Choi, *Science*, 2014, **343**, 990-994.
11. H. Zhang, P. Yilmaz, J. O. Ansari, F. F. Khan, R. Binions, S. Krause and S. Dunn, *Journal of Materials Chemistry A*, 2015, **3**, 9638-9644.
12. Y. Cui, J. Briscoe and S. Dunn, *Chemistry of Materials*, 2013, **25**, 4215-4223.
13. C. Wang, D. Cao, F. Zheng, W. Dong, L. Fang, X. Su and M. Shen, *Chem. Commun.*, 2013, **49**, 3769-3771.
14. H. Kunioku, M. Higashi, O. Tomita, M. Yabuuchi, D. Kato, H. Fujito, H. Kageyama and R. Abe, *Journal of Materials Chemistry A*, 2018, **6**, 3100-3107.
15. D. Kang, Y. Park, J. C. Hill and K.-S. Choi, *The Journal of Physical Chemistry Letters*, 2014, **5**, 2994-2999.
16. E. Zahedi, B. Xiao and M. Shayestefar, *Inorganic Chemistry*, 2016, **55**, 4824-4835.
17. H. S. Park, C.-Y. Lee and E. Reisner, *Physical Chemistry Chemical Physics*, 2014, **16**, 22462-22465.
18. W. Ji, K. Yao, Y.-F. Lim, Y. C. Liang and A. Suwardi, *Applied Physics Letters*, 2013, **103**, 062901.
19. L. Zhang, C. Baumanis, L. Robben, T. Kandiel and D. Bahnemann, *Small*, 2011, **7**, 2714-2720.
20. A. S. Poghossian, H. V. Abovian, P. B. Avakian, S. H. Mkrtchian and V. M. Haroutunian, *Sensors and Actuators B: Chemical*, 1991, **4**, 545-549.
21. Y. Li, Y. Zhang, W. Ye, J. Yu, C. Lu and L. Xia, *New Journal of Chemistry*, 2012, **36**, 1297-1300.
22. Q.-J. Ruan and W.-D. Zhang, *The Journal of Physical Chemistry C*, 2009, **113**, 4168-4173.
23. S. Sun, W. Wang, L. Zhang and M. Shang, *The Journal of Physical Chemistry C*, 2009, **113**, 12826-12831.
24. C. Ederer and N. A. Spaldin, *Physical Review B*, 2005, **71**, 224103.
25. E. Enriquez, A. Chen, Z. Harrell, P. Dowden, N. Koskelo, J. Roback, M. Janoschek, C. Chen and Q. Jia, *Scientific Reports*, 2017, **7**, 46184.
26. A. Kirsch, M. M. Murshed, M. Schowalter, A. Rosenauer and T. M. Gesing, *The Journal of Physical Chemistry C*, 2016, **120**, 18831-18840.
27. Z. Irshad, S. H. Shah, M. A. Rafiq and M. M. Hasan, *Journal of Alloys and Compounds*, 2015, **624**, 131-136.
28. M. G. Walter, E. L. Warren, J. R. McKone, S. W. Boettcher, Q. Mi, E. A. Santori and N. S. Lewis, *Chemical Reviews*, 2010, **110**, 6446-6473.
29. I. D. Baikie, A. C. Grain, J. Sutherland and J. Law, *Energy Procedia*, 2014, **60**, 48-56.
30. D. Cavalcoli and A. Cavallini, *physica status solidi c*, 2010, **7**, 1293-1300.
31. L. Kronik and Y. Shapira, *Surface and Interface Analysis*, 2001, **31**, 954-965.
32. X. Y. Chen, T. Yu, F. Gao, H. T. Zhang, L. F. Liu, Y. M. Wang, Z. S. Li, Z. G. Zou and J.-M. Liu, *Applied Physics Letters*, 2007, **91**, 022114.
33. L. T. Quynh, C. N. Van, Y. Bitla, J.-W. Chen, T. H. Do, W.-Y. Tzeng, S.-C. Liao, K.-A. Tsai, Y.-C. Chen, C.-L. Wu, C.-H. Lai, C.-W. Luo, Y.-J. Hsu and Y.-H. Chu, *Advanced Energy Materials*, 2016, **6**, 1600686-n/a.
34. S. C. Warren, K. Voïtchovsky, H. Dotan, C. M. Leroy, M. Cornuz, F. Stellacci, C. Hébert, A. Rothschild and M. Grätzel, *Nature Materials*, 2013, **12**, 842.
35. A. G. Tamirat, J. Rick, A. A. Dubale, W.-N. Su and B.-J. Hwang, *Nanoscale Horizons*, 2016, **1**, 243-267.
36. H. Dotan, K. Sivula, M. Gratzel, A. Rothschild and S. C. Warren, *Energy & Environmental Science*, 2011, **4**, 958-964.
37. Y. Ma, S. R. Pendlebury, A. Reynal, F. Le Formal and J. R. Durrant, *Chemical Science*, 2014, **5**, 2964-2973.
38. F. Le Formal, K. Sivula and M. Grätzel, *The Journal of Physical Chemistry C*, 2012, **116**, 26707-26720.
39. S. J. A. Moniz, C. S. Blackman, P. Southern, P. M. Weaver, J. Tang and C. J. Carmalt, *Nanoscale*, 2015, **7**, 16343-16353.